# 4

*INJURY BIOMECHANICS RESEARCH*
*Proceedings of the Thirty-Second International Workshop*

# An Experimental Seat for Measuring External Biofidelity in Rear Impacts

Y. Kang[1], K. Moorhouse[2], J. Stammen[3], and J. Bolte IV[1]

*[1] The Ohio State University; [2] Transportation Research Center, Inc.; [3] NHTSA VRTC*



## ABSTRACT

*The goal of this study is to design, construct, and evaluate a seat for measuring/evaluating external biofidelity in rear impact testing on a HYGE sled. In order to compare crash dummies and post-mortem human subjects (PMHS) the seat must be: (1) able to match the seat back rotation response, overall geometry, and padding/upholstery characteristics of a typical OEM seat, (2) capable of measuring how the occupant loads the seat during the event, (3) reusable (i.e., durable enough to withstand multiple tests), and (4) repeatable and reproducible. The geometry and moment-rotation properties of a typical passenger vehicle seat were resolved from the literature. The seat back, seat base, and head restraint were equipped with load cells to measure forces at 20 kHz. Dynamic analysis of a mass-spring-damper arrangement subjected to a moderate-velocity pulse (10.5 g, 24 km/h) was conducted to determine the spring constant K and damping factor C necessary to replicate the motion of a typical seat. Using the results of this analysis, two seats were constructed for attachment to the HYGE sled. A ballast Hybrid III 50th percentile male dummy was placed in each seat, with the load cells measuring the forces applied by the dummy. High speed video and accelerometers were used to verify seat back rotation and for inertial compensation of the load cells. Several sled tests were conducted with progressive versions of the seat until the performance criteria were satisfied. The final version of the seat was able to withstand multiple events without degradation in the repeatability of the seat back rotation response (CV < 5 %) and the two seats were reproducible when compared to one another (CV < 5%). Dynamic analysis of measured forces confirmed that the load cells were able to quantify the occupant loading on the seat. The next phase of this study is to test rear impact dummies and PMHS in this seat to generate internal and external biofidelity data in moderate-velocity conditions for use with the NHTSA Biofidelity Ranking System.*

## INTRODUCTION

The modern rear impact dummies (BioRID II, RID3D) and their predecessors (BioRID P3, RID2) were designed primarily for low speed testing where whiplash injuries generally occur (at or below FMVSS 202 ≈ 18 km/h), and the "internal" biofidelity (i.e., kinematics and internal loads) of the dummies at these low speeds has been evaluated extensively relative to the response of volunteers and PMHS (Davidsson et al., 1999a; Cappon et al., 2000; Cappon et al., 2001; Philippens et al., 2002; Croft & Philippens, 2007). In addition to the internal biofidelity, a few studies also examined the "external" biofidelity (i.e., how the occupant loads the vehicle) of the dummies by measuring the loading on the seat back and/or head restraint using pressure sensing mats or load cells (Davidsson et al., 1999b; Siegmund et al., 2001; Willis et al., 2005). The biofidelity studies above were conducted in many different seat configurations (e.g., rigid bench seats, various production seats, with/without head restraints, etc.) and the common conclusion among them is that both of the rear impact dummies are more biofidelic at these low speeds than the Hybrid III, which is still currently used in the design and evaluation of many OEM seats. However, the moderate-to-high speed (> 18 km/h) biofidelity of the rear impact dummies has not been well-established even though it is important that seat design is optimized to provide sufficient protection to all occupants at all speeds.

Moreover, the utilization of a rear impact dummy which is biofidelic at ΔV > 18 km/h may be more important than previously assumed. The number of people injured in rear impact collisions and the maximum severity of their injuries are shown in Figure 1, where the blue column represents the number of people injured at ΔV ≤ 18 km/h, while the purple column shows the number of people injured at ΔV > 18 km/h. This chart indicates that the frequency of the more common Maximum AIS 1 injuries, such as whiplash, may occur at the moderate and high speeds as often as they occur at speeds equivalent to or below 18 km/h. It can also be seen that the more severe Maximum AIS 2+ and 3 + injuries may be more frequent at ΔV > 18 km/h. Nevertheless, there is currently no dynamic test standard for evaluating the integrity of the seat back/head restraint in response to moderate-to-high speed rear impacts, and the biofidelity of the rear impact dummies at these speeds is relatively unknown.

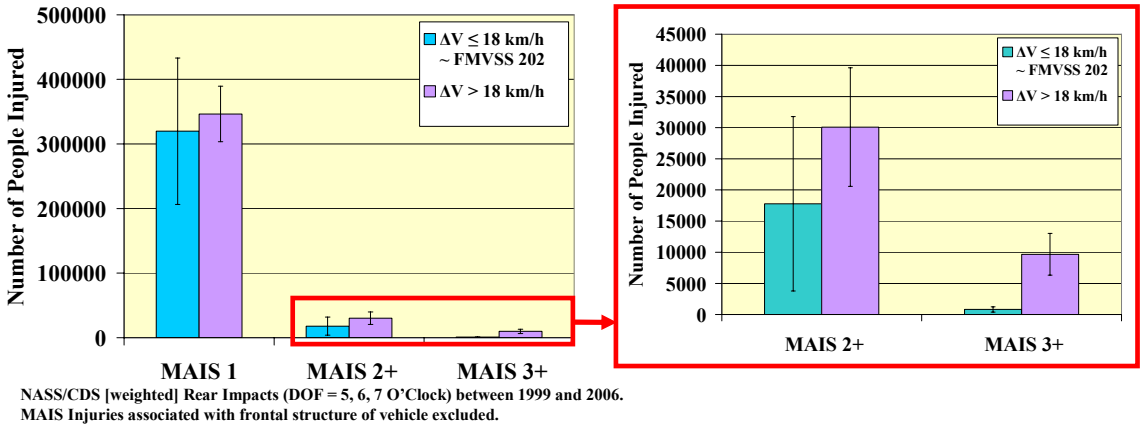


Figure 1: Number and severity of injuries associated with rear impact accidents.

Kim et al. (2003) evaluated the biofidelity of the BioRID II, RID2, and Hybrid III at a higher severity of ΔV = 28 km/h in rigid bench seat conditions, but no tests were conducted in production seats where the seat back was able to yield (i.e., rotate) upon impact. Conversely, a few studies have evaluated the moderate-to-high speed performance of the dummies in various production seats, as well as their ability to distinguish between seat designs, but no direct comparison was made to the response of human subjects (Gotou et al., 2001; Bortenschlager et al., 2003; Kim et al., 2005; Mallory & Stammen, 2007). In fact, only a few studies have examined the human subject response to moderate-to-high speed rear impact (Mertz & Patrick, 1967; Hu et al., 1977; Kallieris et al., 1996; Philippens et al., 2000; Yoganandan et al., 2000), and none of them utilized a modern seat with a 'yielding' seat back and typical padding/upholstery. It is important to understand the human response in these "realistic" test conditions as the kinematics and kinetics of the occupant are expected to be quite different than in the rigid non-rotating seat condition.

Once an understanding of the human response in these test conditions is obtained, the corresponding biofidelity of the rear impact dummies can be assessed.

Therefore, the objective of this study is to design, construct, and evaluate a seat for rear impact testing of PMHS and dummies on a HYGE sled that must satisfy the following criteria necessary for a biofidelity analysis:

1) The seat must be able to match the seat back rotation response, overall geometry, and padding/upholstery characteristics of a typical OEM seat.
2) The seat must contain instrumentation to measure the occupant loading on the seat so that the external biofidelity of the dummies can be assessed.
3) The seat must be reusable (i.e., durable enough to withstand multiple tests) as opposed to typical OEM seats which must be replaced after moderate or high speed impacts.
4) The seat must be repeatable and reproducible.

# METHODS

## Design criteria for matching the seat back rotation response of a typical OEM seat

In order to determine the seat back rotation response of a typical OEM seat, the average rotational stiffness of various OEM seats was obtained from the literature as shown in Figure 2 (Molino, 1998). In the figure, each bar represents the rotational stiffness of a seat from a different vehicle, with the seats on the left side of the chart representing single recliner seats, and the seats on the right side representing dual recliner seats. The average seat back rotational stiffness for all of the seats included in the study was 65 N-m/deg, represented by the red line.

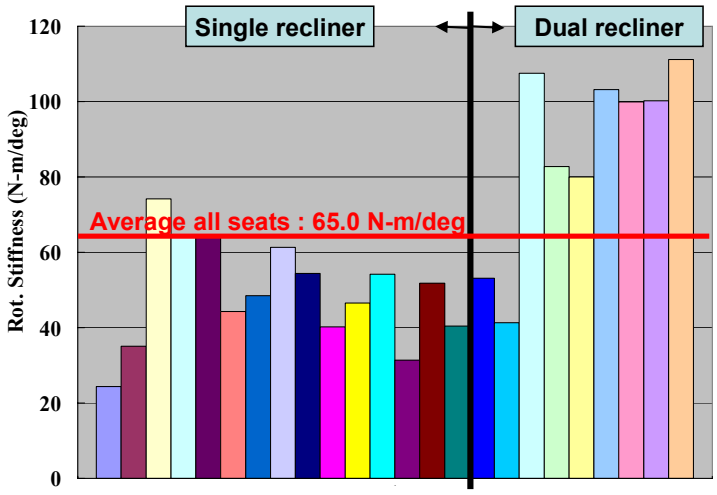


Figure 2: Average rotational stiffness of various OEM seats (Molino, 1998).

A model of a target OEM seat was created to analyze the motion of the seat back during dynamic loading (Figure 3). A target rotational stiffness, $K_{RT}$, of 65 N-m/deg was applied at the pivot of the OEM seat model, and the mass and dimensions of a Hybrid III 50$^{th}$ percentile male dummy were used. It was assumed that the seat back and the upper torso of the dummy were merged as one part to simplify the dynamic analysis. The equation of motion of the target OEM seat model can be defined as shown in Equation (1):

$$J_{SP} \cdot \ddot{\theta}_{SB}(t) = (M_{SB} + M_{dummy}) \cdot g \cdot \{H_{CM} \cdot \sin(\theta_{SB}(t)) - B_{CM} \cdot \cos(\theta_{SB}(t))\} + F(t) \cdot \{H_{CM} \cdot \cos(\theta_{SB}(t)) + B_{CM} \cdot \sin(\theta_{SB}(t))\} - K_{RT} \cdot (\theta_{SB}(t) - \theta_{SBinitial}) \quad (1)$$

where:

$$J_{SP} = M_{SB} \cdot \left(\frac{H^2 + W^2}{12} + \left(\frac{H}{2} + h\right)^2\right) + J_{dummy} + M_{dummy} \cdot (h_{CM}^{\ 2} + b_{CM}^{\ 2}) \quad (2)$$

$$H_{CM} = \frac{M_{SB} \cdot (h + H/2) + M_{dummy} \cdot h_{CM}}{M_{SB} + M_{dummy}} \quad (3)$$

$$B_{CM} = \frac{M_{SB} \cdot 0 + M_{dummy} \cdot b_{CM}}{M_{SB} + M_{dummy}} \quad (4)$$

In Equations (1)-(4), $J_{SP}$ is the moment of inertia of the merged body with respect to the seat pivot point, $H_{CM}$ & $B_{CM}$ are the distances from the seat base and seat back to the center of mass of the merged body, $\theta_{SBInitial}$ = 25 degrees is the initial seat back angle, $J_{dummy}$ is the moment of inertia of the upper torso of the dummy, and $h_{CM}$ & $b_{CM}$ are the distances from the seat base and seat back to the center of mass of the dummy upper torso.

The remainder of the variables in Equations (1)-(4) are defined in Figure 3. The distance used from the hip joint to the upper torso CM was 0.35 m based on the Hybrid III 50th percentile male dummy, and the distance used from the seat base and seat back to the hip joint were 0.086 m and 0.137 m, respectively. Table 1 provides other dimensions and mass properties used in the dynamic analysis.

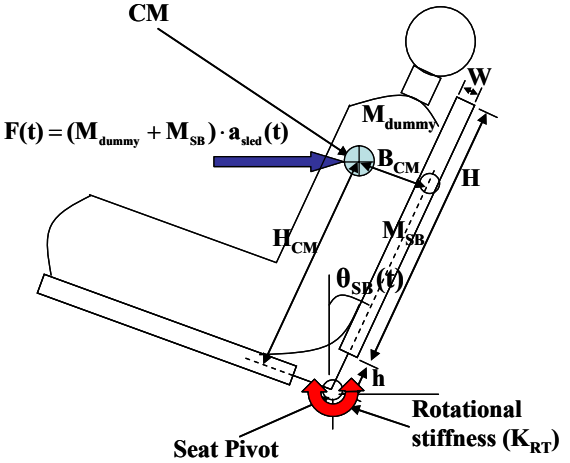


CM: center of mass of the merged body
F(t): inertial force of sled pulse
$M_{dummy}$ : mass of upper torso of dummy
$M_{SB}$ : mass of seat back
$a_{sled}$ : applied sled acceleration pulse
$H_{CM}$ : distance from seat base to CM
$B_{CM}$ : distance from seat back to CM
$\theta_{SB}(t)$ : seat back angle
H : height of seat back
W : width of seat back
$K_{RT}$ : rotational stiffness at the seat pivot
h : distance from seat pivot to bottom of seat back

Figure 3: Model of a target OEM seat.

Table 1. Dimensions and mass properties for the OEM seat.

| | | | |
|---|---|---|---|
| H [m] | 0.508 | $h_{CM}$ [m] | 0.461 |
| W[m] | 0.051 | $b_{CM}$ [m] | 0.162 |
| h [m] | 0.051 | $M_{SB}$ [kg] | 5.1 |
| $H_{CM}$ [m] | 0.444 | $M_{dummy}$ [kg] | 40 |
| $B_{CM}$ [m] | 0.144 | $J_{dummy}$ [kg-m$^2$] | 5 |
| | | $J_{SP}$ [kg-m$^2$] | 15.155 |

The dynamic input applied to the OEM seat model was a moderate acceleration pulse with a magnitude of 10.5 g and duration of 100 ms as shown in Figure 4(a), resulting in an approximate ΔV of 24 km/h. The model simulation produced the seat back rotation shown in Figure 4(b) with a maximum rotation angle of approximately 32 degrees. Note that seat back rotation in Figure 4(b) is defined as motion of the seat beyond the initial angle of the seat back , $\theta_{SBInitial}$ = 25 degrees, so a final rotation angle of 32 degrees is equivalent to a final seat back angle of 57 degrees. This maximum rotation angle was found to be consistent with what has been reported in previous studies as shown in Figure 5, where each bar represents the maximum seat back rotation at ΔV = 24 km/h for a production seat from the literature, and the maximum rotation of our OEM seat model is expressed by the red line. Therefore, the results from the dynamic analysis of the target OEM seat model (i.e., 32 degrees of maximum rotation given the input acceleration pulse applied) were used as the performance requirement for development of the experimental seat.

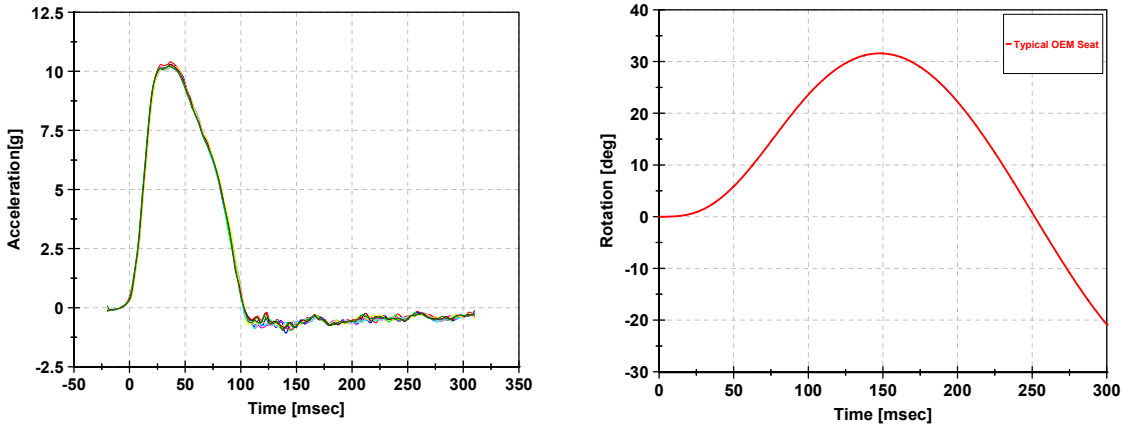


(a) Input: Acceleration Pulse (b) Output: Seat Back Rotation

Figure 4: Dynamic input acceleration pulse and output seat back rotation of the OEM model.

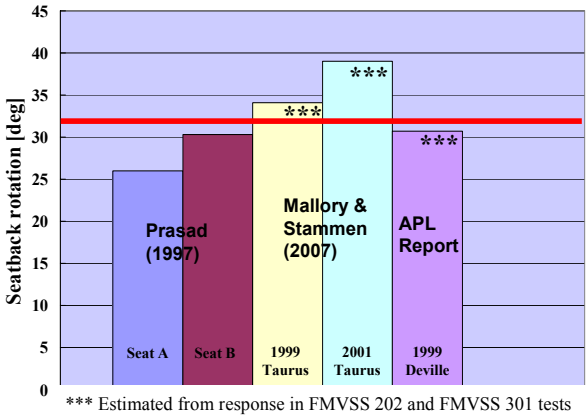


*** Estimated from response in FMVSS 202 and FMVSS 301 tests

Figure 5: Average maximum seat back rotation from the literature (ΔV = 24 km/h).

## Dynamic analysis for development of the experimental seat

An experimental seat was constructed and instrumented with uni-axial load cells to measure the occupant loading on the seat during impact (Figure 6). The seat instrumentation included two load cells in the head restraint, six load cells in the seat back, and four load cells in the seat base. This load cell arrangement was chosen in order to adequately measure the spatial distribution of the occupant loading at a sample rate sufficient for a moderate-to-high speed rear impact event (i.e., 20 kHz). In contrast, using a

dynamic pressure sensing mat, rather than load cells, would typically allow for greater spatial resolution of the distributed loading, but at a sample rate much too low to fully capture the loading profile. The uni-axial load cells were connected to load cell plates (depicted in Figure 6) intended to interact with the occupant through the seat cushions during impact. In order to simplify the design as well as ensure a repeatable seat back rotation response for the experimental seat, it was decided to implement a translational spring-damper system to mimic the seat back recliner mechanism of the target OEM seat (i.e., constant rotational stiffness of 65 N-m/deg at the seat pivot point), as shown in Figure 7. However, since the mass of the proposed experimental seat (29.5 kg) was much greater than that of the target OEM seat (5.1 kg) due to the addition of load cells, load cell plates, and steel framing sturdy enough to support the instrumentation, the actual stiffness required for the experimental seat would be significantly greater in order to achieve similar seat back motion. A dynamic analysis was performed in order to develop an equation of motion and determine a linear spring constant, K, linear damping factor, C, and position for the support pivot, L, for the experimental seat to achieve similar seat back rotation as the target OEM seat, as described below.

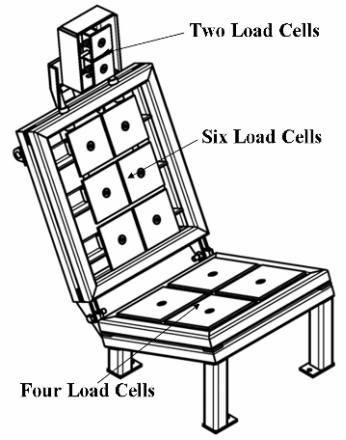


Figure 6: Seat instrumentation for measuring occupant loading during impact.

In short, the goal of this dynamic analysis was to determine values for K and C to achieve similar seat back rotation as the target OEM seat, given the same input acceleration pulse. It was also desired to choose a realistic value of L (shown in Figure 7) relative to the height of the seat back, where the pivots on both the seat back and the sled are frictionless and free to rotate but not translate. The seat back and the upper torso of the dummy were lumped together as one body for the dynamic analysis. Dimensions and mass properties used for the experimental seat are provided in Table 2. Since the mass of the seat back increased from 5.1 kg to 29.6 kg for the experimental seat due to addition of the instrumentation, the moment of inertia and location of the merged body center of mass (i.e., $H_{CM}$ and $B_{CM}$) changed since they are dependent on the seat back mass. Most of the remaining dimensional parameters for the experimental seat (Table 2) are the same as for the target OEM seat (Table 1).

Figure 8 and Equations (5)-(7) illustrate the geometric relationship between the parameters $\{l, w_1, w_2\}$ and $\{L, D, \theta_{SB}(t)\}$ for the proposed experimental seat system.

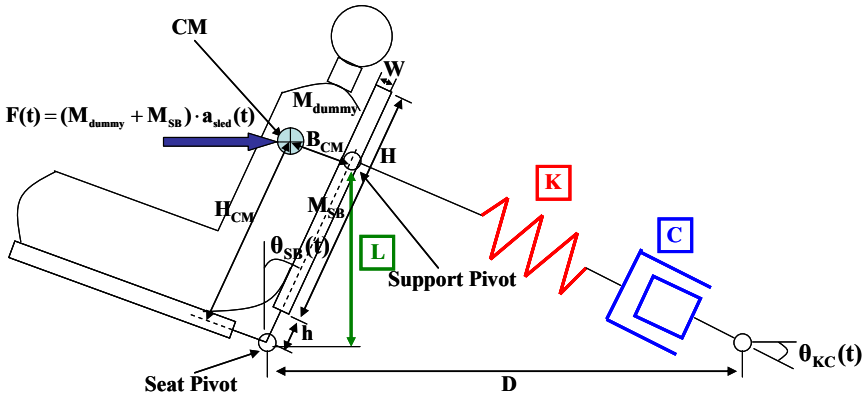


Figure 7: Experimental seat system used for dynamic analysis.

Table 2. Dimensions and mass properties for experimental seat system.

| | | | |
|---|---|---|---|
| H [m] | 0.508 | $h_{CM}$ [m] | 0.461 |
| D [m] | 1.138 | $b_{CM}$ [m] | 0.162 |
| W[m] | 0.051 | $M_{SB}$ [kg] | 29.6 |
| h [m] | 0.051 | $M_{dummy}$ [kg] | 40 |
| $H_{CM}$ [m] | 0.395 | $J_{dummy}$ [kg-m$^2$] | 5 |
| $B_{CM}$ [m] | 0.093 | $J_{SP}$ [kg-m$^2$] | 17.963 |

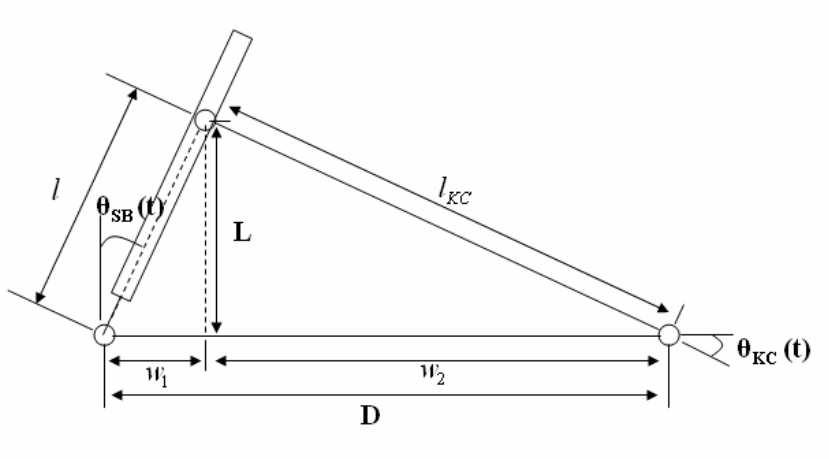


Figure 8: Geometric relationship of experimental seat system parameters.

$$l = \frac{\mathbf{L}}{\cos(\theta_{SBinitial})} \tag{5}$$

$$w_1 = l \cdot \sin(\theta_{SB}(t)) \tag{6}$$

$$\begin{aligned} w_2 &= \mathbf{D} - w_1 \\ &= \mathbf{D} - l \cdot \sin(\theta_{SB}(t)) \end{aligned} \tag{7}$$

The length ( $l_{KC}$ ) of the spring-damper and its first time derivative ( $\dot{l}_{KC}$ ) are as follows:

$$l_{KC} = \sqrt{l^2 + \mathbf{D}^2 - 2l \cdot \mathbf{D} \cdot \cos(\frac{\pi}{2} - \theta_{SB}(t))} = \sqrt{l^2 + \mathbf{D}^2 - 2l \cdot \mathbf{D} \cdot \sin(\theta_{SB}(t))} \tag{8}$$

$$\dot{l}_{KC} = \frac{-l \cdot \mathbf{D} \cdot \cos(\theta_{SB}(t))}{\sqrt{l^2 + \mathbf{D}^2 - 2l \cdot \mathbf{D} \cdot \sin(\theta_{SB}(t))}} \cdot \dot{\theta}_{SB}(t) \tag{9}$$

In the experimental seat system, $\theta_{KC}(t)$ is dependent on $\theta_{SB}(t)$, and their relationship can be expressed as in Equation (10):

$$\tan(\theta_{KC}(t)) = \frac{l \cdot \cos(\theta_{SB}(t))}{\mathbf{D} - l \cdot \sin(\theta_{SB}(t))} \quad \Rightarrow \quad \theta_{KC}(t) = \tan^{-1}(\frac{l \cdot \cos(\theta_{SB}(t))}{\mathbf{D} - l \cdot \sin(\theta_{SB}(t))}) \tag{10}$$

Figure 9 shows a free body diagram (FBD) for the proposed experimental seat system where $d_1$, $d_2$, $d_3$, and $d_4$ are distances from the seat pivot to each external force which can be expressed as shown in Equations (11)-(14).

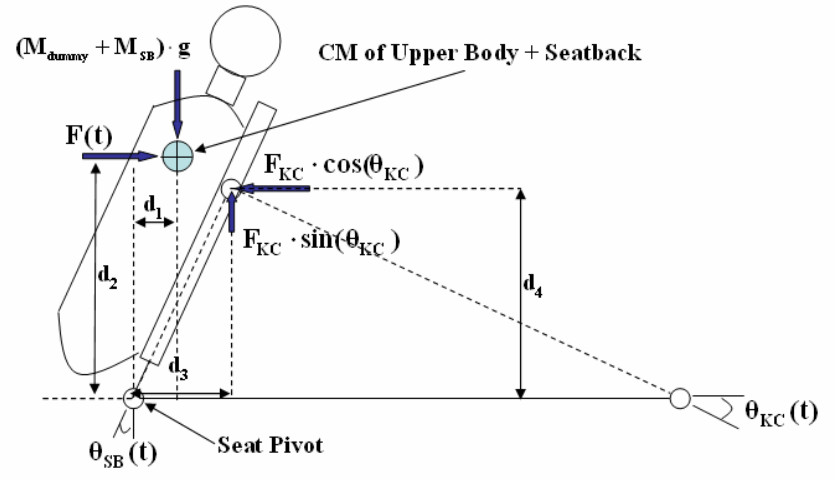


Figure 9: Free body diagram for the experimental seat system.

$$\mathbf{d}_1 = \mathbf{H}_{CM} \cdot \sin(\theta_{SB}(t)) - \mathbf{B}_{CM} \cdot \cos(\theta_{SB}(t)) \tag{11}$$

$$\mathbf{d}_2 = \mathbf{H}_{CM} \cdot \cos(\theta_{SB}(t)) + \mathbf{B}_{CM} \cdot \sin(\theta_{SB}(t)) \tag{12}$$

$$\mathbf{d}_3 = \frac{\mathbf{L}}{\cos(\theta_{SBinitial})} \cdot \sin(\theta_{SB}(t)) \tag{13}$$

$$\mathbf{d}_4 = \frac{\mathbf{L}}{\cos(\theta_{SBinitial})} \cdot \cos(\theta_{SB}(t)) \tag{14}$$

The external moment equation calculated around the seat pivot is as follows:

$$\begin{aligned}\sum \mathbf{M}_{\text{seat pivot}} &= (\mathbf{M}_{\text{SB}} + \mathbf{M}_{\text{dummy}}) \cdot \mathbf{g} \cdot \{\mathbf{H}_{\text{CM}} \cdot \sin(\theta_{\text{SB}}(t)) - \mathbf{B}_{\text{CM}} \cdot \cos(\theta_{\text{SB}}(t))\} \\ &+ \mathbf{F}(t) \cdot \{\mathbf{H}_{\text{CM}} \cdot \cos(\theta_{\text{SB}}(t)) + \mathbf{B}_{\text{CM}} \cdot \sin(\theta_{\text{SB}}(t))\} \\ &- \frac{\mathbf{L}}{\cos(\theta_{\text{SBinitial}})} \times \mathbf{F}_{\text{KC}} \cdot \{\cos(\theta_{\text{KC}}(t)) \cdot \cos(\theta_{\text{SB}}(t)) + \sin(\theta_{\text{KC}}(t)) \cdot \sin(\theta_{\text{SB}}(t))\}\end{aligned} \tag{15}$$

where F(t) is the applied force with respect to the center of mass of the merged body, and $F_{KC}$ is the spring-damper reaction force which can be obtained using Equation (16)

$$\begin{aligned}\mathbf{F}_{\text{KC}} &= \mathbf{K} \cdot \boldsymbol{\delta} + \mathbf{C} \cdot \dot{\boldsymbol{\delta}} \\ &= \mathbf{K} \cdot (l_{KC0} - l_{KC}) + \mathbf{C} \cdot (\dot{l}_{KC0} - \dot{l}_{KC})\end{aligned} \tag{16}$$

where $l_{KC}$ and its first time derivative were previously defined in Equations (8) and (9), and $l_{KC0}$ and its first time derivative are calculated at the initial position and velocity of the seat back.

Finally, the resulting equation of motion for the experimental seat system is shown in Equation (17):

$$\begin{aligned}\mathbf{J}_{\text{SP}} \cdot \ddot{\boldsymbol{\theta}}_{\text{SB}}(t) &= (\mathbf{M}_{\text{SB}} + \mathbf{M}_{\text{dummy}}) \cdot \mathbf{g} \cdot \{\mathbf{H}_{\text{CM}} \cdot \sin(\theta_{\text{SB}}(t)) - \mathbf{B}_{\text{CM}} \cdot \cos(\theta_{\text{SB}}(t))\} \\ &+ \mathbf{F}(t) \cdot \{\mathbf{H}_{\text{CM}} \cdot \cos(\theta_{\text{SB}}(t)) + \mathbf{B}_{\text{CM}} \cdot \sin(\theta_{\text{SB}}(t))\} \\ &- \frac{\mathbf{L}}{\cos(\theta_{\text{SBinitial}})} \times \mathbf{F}_{\text{KC}} \cdot \cos(\theta_{\text{SB}}(t) - \theta_{\text{KC}}(t))\end{aligned} \tag{17}$$

where

$$\mathbf{F}(t) = (\mathbf{M}_{\text{SB}} + \mathbf{M}_{\text{dummy}}) \cdot \mathbf{a}_{\text{sled}} \tag{18}$$

$$\begin{aligned}\mathbf{F}_{\text{KC}} &= \mathbf{K} \cdot (\sqrt{l^2 + \mathbf{D}^2 - 2l \cdot \mathbf{D} \cdot \sin(\theta_{\text{SBinitial}})} - \sqrt{l^2 + \mathbf{D}^2 - 2l \cdot \mathbf{D} \cdot \sin(\theta_{\text{SB}}(t))}) \\ &+ \mathbf{C} \cdot \left(\frac{-l \cdot \mathbf{D} \cdot \cos(\theta_{\text{SBinitial}})}{\sqrt{l^2 + \mathbf{D}^2 - 2l \cdot \mathbf{D} \cdot \sin(\theta_{\text{SBinitial}})}} \cdot \dot{\theta}_{\text{SBinitial}} - \frac{-l \cdot \mathbf{D} \cdot \cos(\theta_{\text{SB}}(t))}{\sqrt{l^2 + \mathbf{D}^2 - 2l \cdot \mathbf{D} \cdot \sin(\theta_{\text{SB}}(t))}} \cdot \dot{\theta}_{\text{SB}}(t)\right)\end{aligned} \tag{19}$$

$$\theta_{\text{KC}}(t) = \tan^{-1}\left(\frac{l \cdot \cos(\theta_{\text{SB}}(t))}{\mathbf{D} - l \cdot \sin(\theta_{\text{SB}}(t))}\right) \tag{20}$$

Equation (17) was solved numerically (4th or 5th Runge-Kutta method, MATLAB) using an iterative parametric approach whereby K, C, and L were varied, and the resulting seat back kinematics were determined and compared to results from the target OEM seat model. The initial position and velocity of the seat back were 25 degrees and 0 deg/sec, respectively. It was assumed that realistic values of L had a lower boundary, L0, and an upper boundary, L10, where L0 is the distance from the pivot point to the midpoint of the seat back and L10 is the distance from the pivot point to the top of the seat back. It was found that for any non-zero value of the damping factor, C, there was a significant response delay which made it impossible for the seat back motion of the experimental seat to closely match that of the target OEM seat. Therefore, the damping term was set to zero and for each of the eleven L values, the stiffness coefficient of the translational spring was determined that resulted in a maximum seat back rotation angle of 32 ± 0.1 degrees. These results for each of the eleven values of L are listed in Table 3. Each of the values obtained for K at the various attachment points were appropriate to adequately match the motion of the target OEM seat as shown in Figure 10, although small differences in the motion time-history between the two seats appeared due to the differing merged body centers of mass and the different operational principles of the recliner mechanisms. A stiffness of 27,000 N/m at the L7 location was selected because

the seat back and spring were perpendicular to each other in the middle of the rearward motion when attached at L7.

Table 3. Required spring stiffness values for each attachment point on seat back.

| | *l* [inch] | L [m] | K[N/m] |
|---|---|---|---|
| L0 | 12 | 0.276 | 76700 |
| L1 | 13 | 0.299 | 64000 |
| L2 | 14 | 0.322 | 54300 |
| L3 | 15 | 0.345 | 46400 |
| L4 | 16 | 0.368 | 40000 |
| L5 | 17 | 0.391 | 34800 |
| L6 | 18 | 0.414 | 30500 |
| L7 | 19 | 0.437 | 27000 |
| L8 | 20 | 0.460 | 24000 |
| L9 | 21 | 0.483 | 21500 |
| L10 | 22 | 0.506 | 19200 |

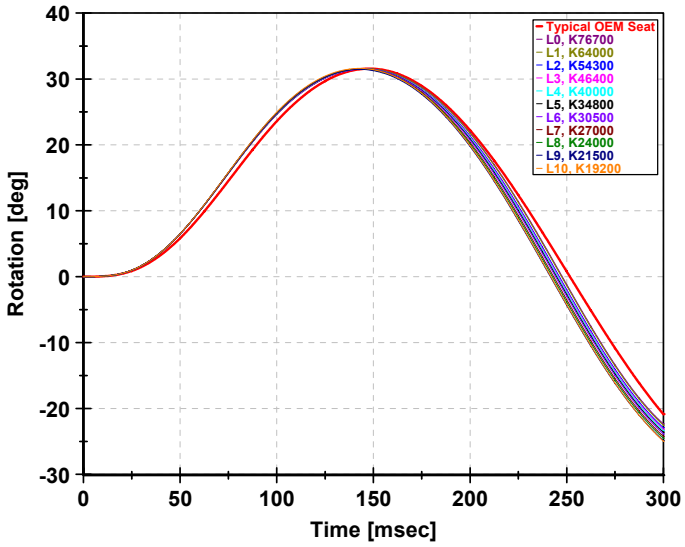


Figure 10: Comparison of seat back motion for experimental seat (L0~L10) and target OEM seat.

Even though no damping was required during the rearward motion of the seat, a one-way damper acting only during rebound was installed to keep the spring from thrusting the seat back forward after maximum rotation, and potentially ejecting the occupant. Figure 11 shows the principle idea behind the one-way damper system which is essentially a step function whereby no damping force is generated during rearward motion, but is activated at $t_{max}$ (i.e., time of maximum seat back rotation). Figure 12 shows the seat back angle response for various levels of one-way damping using a stiffness of 27,000 N/m and attachment point L7. In order to achieve the one-way damping mechanically, a telescoping tube and spring-loaded slide bolt arrangement was implemented in series with an adjustable damper that was rigidly attached to the lower half of the telescoping tube (Figure 13). During rearward motion, the upper half of the telescoping tube slides into the lower half with little resistance. Once the maximum rotation of the seat back is reached, the spring-loaded slide bolt attached to the lower half drops into the hole on the upper half locking the telescoping tubes together and thus engaging the damper for the rebound phase.

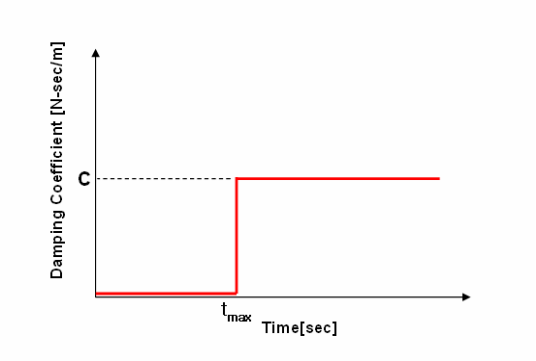


Figure 11: Step function representing the one-way damper.

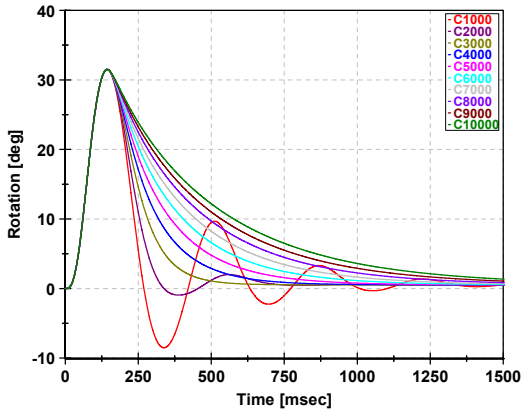


Figure 12: Seat back motion for various levels of damping (K = 27,000 N/m; L = L7).

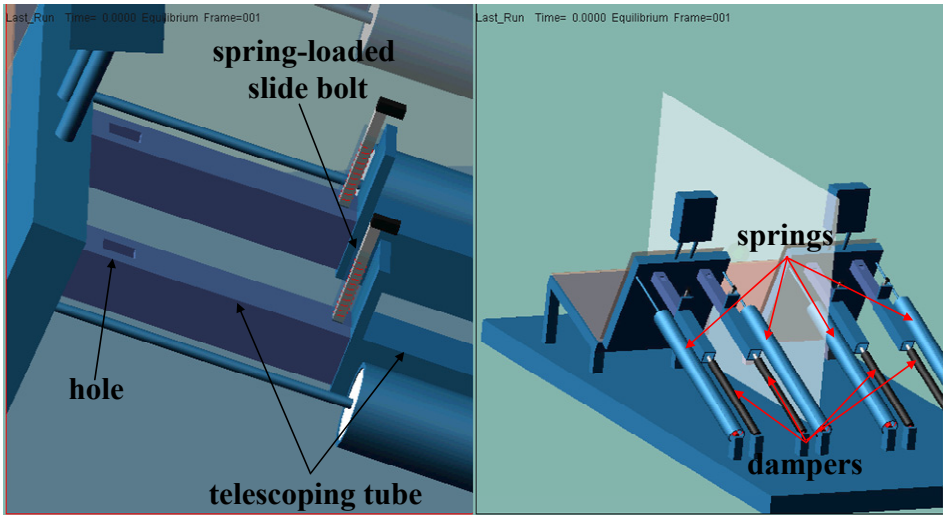


Figure 13: Telescoping tube and spring-loaded slide bolt arrangement to achieve one-way damping.

## Final design description for experimental seats and seat evaluation test plan

Figure 14 highlights the features for the final seat design. The head restraint mass is 5.5 kg with a support bar diameter of 17 mm, and the head restraint height is infinitely adjustable using set screws. The dimensions of the head restraint are representative of a typical OEM seat. Based on the dynamic analysis, two parallel adjustable one-way dampers (Ace Controls, Inc., Farmington, MI) and two parallel springs (The Yost Superior Co., Springfield, OH) with stiffness values of 13,500 N/m (i.e., half of 27000 N/m) were installed. The geometry of the seat is similar to that of a typical OEM seat, and the padding, cushions and seat cover are from a 1999 Toyota Camry seat. As previously discussed, the seat includes a total of 12 uni-axial load cells (Transducer Techniques, Temecula, CA) to measure the occupant loading on the seat (two in the head restraint, six in the seat back, and four in the seat base).

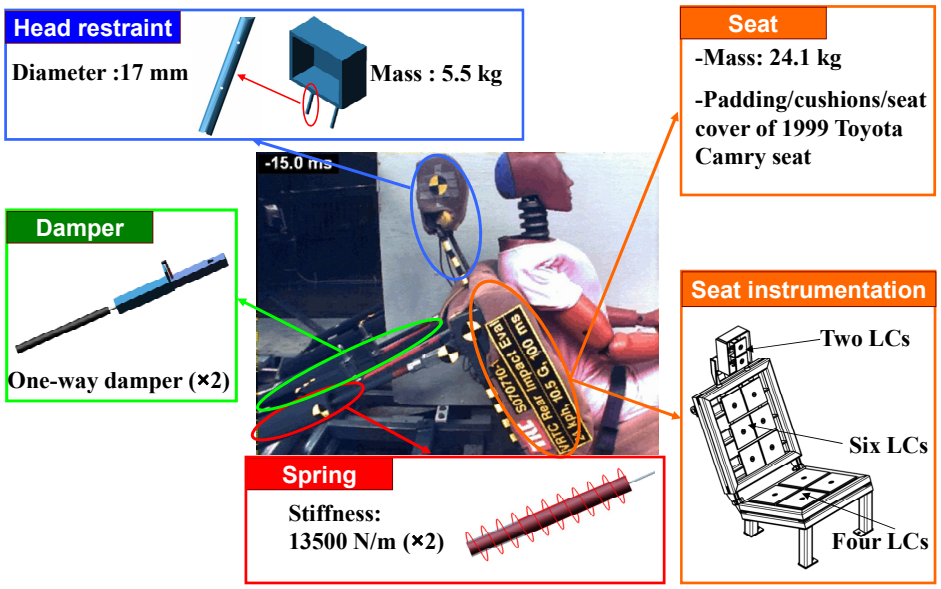


Figure 14: Description of final seat design.

Figure 15 shows the sled buck configuration chosen for the experimental seats, where two seats were placed side-by-side so that each sled test would produce two occupant exposures. Seat back rotation and performance of the spring-damper assembly were recorded at 1500 frames/sec using high speed digital cameras traveling with the sled. Accelerometers were installed on the seat backs for inertial compensation of the load cells and for a redundant measure of seat back rotation.

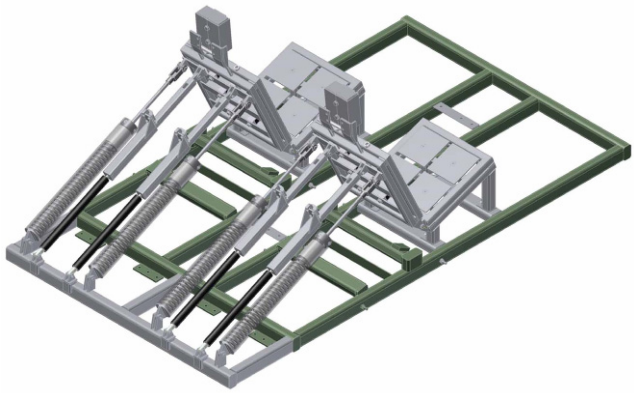

Figure 15: Sled buck configuration for the experimental seats.

# RESULTS

## Initial seat evaluation test results

Two initial sled tests (10.5g and ΔV = 24 km/h) were conducted using ballast Hybrid III 50$^{th}$ percentile dummies to document the performance of the seats with respect to durability, function of the spring-damper assemblies, and the ability of the seats to match the seat back rotation predicted by the model. For this initial test series, the high speed video cameras focused on performance of the spring-damper assembly for the seat in the driver position, and were used to measure seat back rotation for the seat in the passenger position. For the two tests, the experimental seats appeared durable without any noticeable damage to any of the components, and the spring-damper assemblies functioned as intended. The seat back

rotation response for the seat in the passenger position is shown in Figure 16. The seat back rotation was similar to what was predicted by the dynamic analysis. The rotation response differed slightly from the model simulation (Figure 10), likely due to the model assumption that the seat back and the upper torso of the dummy are merged as one body. It is important to note that the dummies in this test series were used only as ballast so no effort was made to position them in a repeatable manner. Nevertheless, the repeatability of the seat performance appeared acceptable as can be seen in Figure 16, although this could not be quantified since only two tests were conducted in this initial test series.

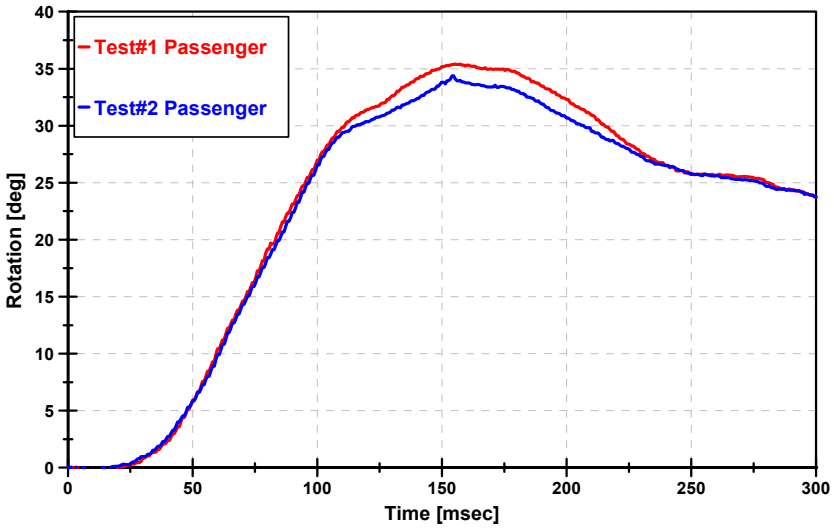


Figure 16: Seat back rotation for the passenger seat in initial test series (10.5 g, ΔV = 24 km/h).

## Additional seat evaluation test results

Once the performance of the seat design was deemed acceptable, another sled test series using the BioRIDII, RID3D and Hybrid III 50$^{th}$ percentile male dummies in the newly designed seats was conducted. The test series consisted of 9 tests / 18 exposures (3 repeated tests x 3 dummies x 2 seats) using the same sled pulse (10.5 g, 24 km/h). In this series it was crucial that the dummies were seated in a repeatable manner and that the seated position of each dummy was the same to enable a direct comparison of response data. Therefore, the H-point location of the seat was determined (OSCAR) since each dummy has its own standard seating procedure relative to the seat H-point. The seating procedure for each dummy was followed within allowable tolerances until the head was level (within ± 0.5 deg) and the backset (i.e., horizontal distance between the back of the head and the front of the head restraint) was 50 ± 5 mm. The head restraint was then adjusted so that the vertical distance between the head CG and the top of the head restraint was 80 ± 5 mm. Specific landmarks required during the dummy positioning procedures were digitized using a Faro Arm (Faro Arm Technologies, Lake Mary FL).

This test series was just recently completed and the data has yet to be fully analyzed so results regarding comparison of the dummy responses will be reported elsewhere. Therefore, only results relevant to the performance of the seat using the Hybrid III will be discussed in this manuscript (e.g., durability of the seats, ability to match the seat back rotation predicted by the model, repeatability and reproducibility of the seat back rotation response and instrumentation integrity). The durability of the spring-damper arrangements was found to be adequate, although some minor bending in the damper rods was observed which will be addressed prior to any future test series. The seat back rotation response for the six tests involving the Hybrid III are shown in Figure 17, where the red, blue and green curves represent the seat in the driver position, and the pink, light blue, and light green curves represent the seat in the passenger position. The seat back rotation was again similar to that predicted by the model. The coefficient of variation (CV) was calculated for each point in time within the shaded region in Figure 17 and then averaged to assess the repeatability of each seat and the reproducibility between the two seats. The

resulting CV scores were 3.9 % for driver seat repeatability, 2.5 % for passenger seat repeatability, and 4.4 % for reproducibility between the two seats. These results indicate that for the tests involving the Hybrid III the experimental seat exhibited 'excellent' repeatability and reproducibility since NHTSA has historically categorized CV scores of 0-5% as 'excellent'. Sample data from one of the tests for each seat load cell is shown in Figure 18, where purple, blue, and green areas represent responses from the head restraint, seat back, and seat base, respectively. It appears that this load cell configuration is capable of adequately measuring the occupant loading on the seat as well as the distribution of loading.

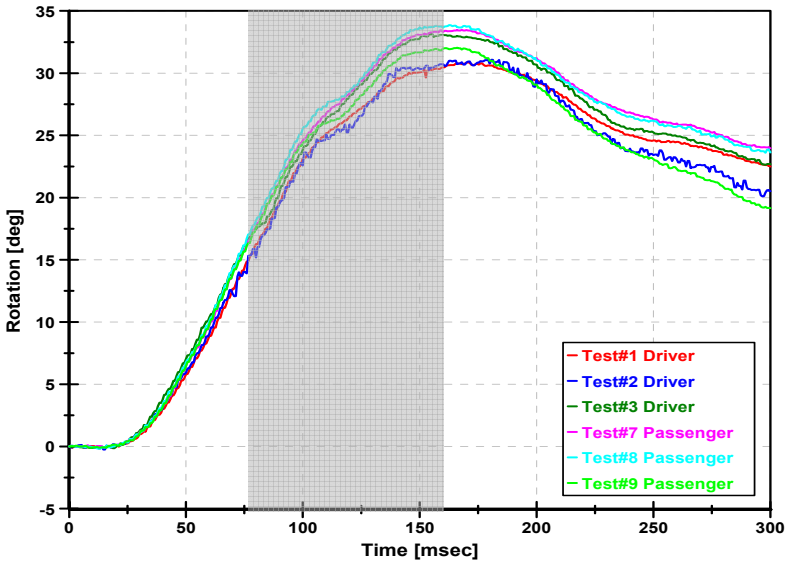


Figure 17: Seat back rotation response for the Hybrid III tests in the rear impact dummy test series.

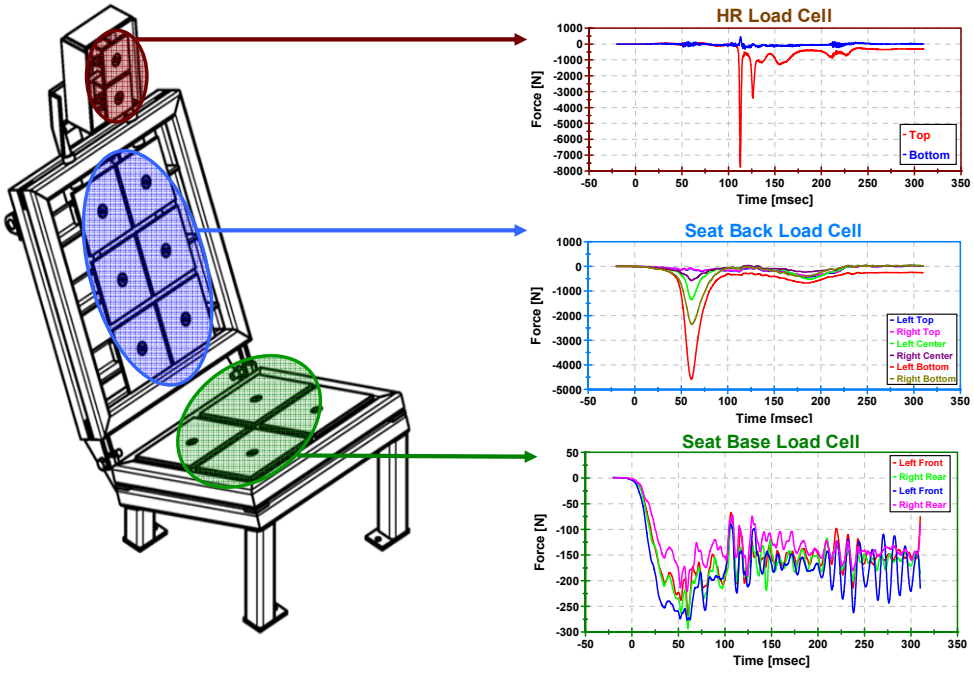


Figure 18: Sample data from seat load cells.

## CONCLUSIONS

An experimental seat for measuring external biofidelity has been designed, constructed, and evaluated by conducting sled tests in moderate-severity rear impact conditions of 10.5 g, 24 km/h. In order to determine the appropriate parameters for the recliner mechanism of the seat (i.e., spring constant, damping factor, and location of the spring-damper attachment), a numerical model was created and simulated under the moderate-severity conditions. The experimental seat was able to match the motion of a typical OEM seat for the pulse applied with a maximum seat back rotation angle of approximately 32 degrees, as the dynamic analysis of the model predicted. One-way dampers were designed and installed to control the rebound motion of the seat. The seat includes instrumentation to measure the occupant loading on the seat including two load cells in the head restraint, six load cells in the seat back, and four load cells in the seat base. These can be used to determine the distributed loading of the occupant, while being sampled at a sufficiently high rate for a moderate-to-high speed rear impact event (i.e., 20 kHz). Data from these load cells can be used to determine the seat loading for PMHS necessary to assess the external biofidelity of the rear impact dummies. The seat was able to withstand multiple events with 'excellent' repeatability and reproducibility (CV < 5 %).

The next step in this research is to conduct further sled tests using rear impact dummies (i.e., BioRIDII and RID3D) and PMHS. For the PMHS sled tests, a new instrumentation technique will be developed for instrumenting the anterior aspect of each of the cervical vertebral bodies for evaluation of the detailed kinematics. An algorithm that will combine the responses from the seat load cells into a single measure of external biofidelity for each seat region will be developed. Finally, NHTSA's BioRank system will be used to assess the internal and external biofidelity of the rear impact dummies under moderate speed conditions.

## ACKNOWLEDGEMENTS

This research was completed under DOT/NHTSA contract (DTNH22-03-D-08000). The authors would like to thank Jim Clevenger and Rick Waldeck from the Transportation Research Center, Inc. for their support in this project.

## REFERENCES

BORTENSCHLAGER, K., KRAMBERGER, D., BARNSTEINER, K., HARTLIEB, M., FERDINAND, L., LEYER, H., MUSER, M., and SCHMITT, K.-U. (2003). Comparison tests of BioRID II and RID2 with regard to repeatability, reproducibility and sensitivity for assessment of car seat protection potential in rear-end impacts. Proc. 47th Stapp Car Crash Conference, SAE Paper No. 2003-22-0021, 473-488.

CAPPON, H.J., PHILIPPENS, M.M.G.M., VAN RATINGEN, M.R., and WISMANS, J.S.W.M. (2000). Evaluation of Dummy Behaviour during Low Severity Rear Impact. Proc. IRCOBI Conference 2000, 53-66.

CAPPON, H., PHILIPPENS, M., VAN RATINGEN, M., and WISMANS, J. (2001). Development and evaluation of a new rear-impact crash dummy: The RID 2. Proc. 45th Stapp Car Crash Conference, SAE Paper No. 2001-22-0010.

CROFT, A. and PHILIPPENS, M. (2007). The RID2 biofidelic rear impact dummy: A pilot study using human subjects in low speed rear impact full scale crash tests. J. Accident Analysis and Prevention, 39, 340-346.

DAVIDSSON, J., FLOGARD, A., LOVSUND, P., and SVENSSON, M. Y. (1999a). BioRID P3- Design and performance compared to Hybrid III and volunteers in rear impacts at ΔV=7 km/h. Proc. Proc. 43rd Stapp Car Crash Conference, SAE Paper No. 99SC16.

DAVIDSSON, J., LOVSUND, P., ONO, K., SVENSSON, M. Y., and INAMI S. (1999b). A comparison between volunteer, BioRID P3 and Hybrid III performance in rear impacts. Proc. IRCOBI Conference 1999, 165-178.

GOTOU, T., ONO, K., ITO, M., and MATUOKA, F. (2001). A comparison between BioRID AND Hybrid III head/neck/torso response in middle speed sled rear impact tests. Proc. 17th International Technical Conference on the Enhanced Safety of Vehicles, Paper No.116.

HU, A. S., BEAN, S. P., and ZIMMERMAN, R. M. (1977). Response of belted dummy and cadaver to rear impact. Proc. 21st Stapp Car Crash Conference, SAE Paper No. 770929.

KALLIERIS, D., RIZZETTI, A., MATTERN, R., THUNNISSEN,J., and PHILIPPENS, M. (1996). Cervical human spine loads during traumatomechanical investigations. Proc. IRCOBI Conference 1996, 89-106.

KIM, A., SUTTERFIELD, A., RAO, A., ANDERSON, K.F., BERLINER, J., HASSAN, J., IRWIN, A., JENSEN, J., KLEINERT, J., MERTZ, H.J., PIETSCH, H., ROUHANA, S., and SCHERER, R. (2005). A Comparison of the BioRID II, Hybrid III, and RID2 in Low-Severity Rear Impacts. Proceedings of the 19th International Technical Conference of the Enhanced Safety of Vehicles, Paper No. 05-0225

KIM, A., ANDERSON, K. F., BERLINER, J., HASSAN, J., JENSEN, J., MERTZ, H. J., PIETSCH, H., RAO, A., SCHERER, R., and SUTTERFIELD, A. (2003). A biofidelity evaluation of the BioRID II, Hybrid III and RID2 for use in rear impacts. Proc. 47th Stapp Car Crash Conference, SAE Paper No. 2003-22-0022, 489-523.

MALLORY, A. and STAMMEN, J. (2007). Comparative evaluation of rear impact dummies static seat interaction and dynamic testing. NHTSA Docket No. 2007-27986-19.

MERTZ, H. J. and PATRICK, L. M. (1967). Investigation of the kinematics and kinetics of whiplash. Proc. 11th Stapp Car Crash Conference, SAE Paper No. 670919.

MOLINO, L. (1998). Determination of moment-deflection characteristics of automobile seat backs. NHTSA Docket No. 1998-4064-26.

PHILIPPENS, M., WISMANS, J., CAPPON, M., YOGANANDAN, N., and PINTAR, F. (2000). Whole body kinematics using post mortem human subjects in experimental rear impact. Proc. IRCOBI Conference 2000, 363-378.

PHILIPPENS, M., CAPPON, M., VAN RATINGEN, WISMANS, J., SVENSSON, M., SIREY, F., ONO, K., NISHIMOTO, N., and MATSUOKA, F. (2002). Comparison of the rear impact biofidelity of BioRID II and RID2. Proc. 46th Stapp Car Crash Conference, SAE Paper No. 2002-22-0023, 461-476.

PRASAD, P., KIM, A., WEERAPPULI, D.P.V., ROBERTS, V., and SCHNEIDER, D. (1997). Relationships Between Passenger Car Seat Back Strength and Occupant Injury Severity in Rear End Collisions: Field and Laboratory Studies. Proc. 41st Stapp Car Crash Conference, SAE Paper No. 973343, 417-449.

SIEGMUND, G.P., HEINRICHS, B. E., and LAWRENCE, J. M. (2001). Kinetic and kinematic responses of the RID 2a, Hybrid III and Human Volunteers in low-speed rear-end collisions. Proc. 45th Stapp Car Crash Conference, SAE Paper No. 2001-22-0011.

WILLIS, C., CARROLL, J., and ROBERTS, A. (2005). An evaluation of a current rear impact dummy against human response corridors in both pure and oblique rear impact. Proceedings of the 19th International Technical Conference of the Enhanced Safety of Vehicles, Paper No. 05-0061.

YOGANANDAN, N., PINTAR, F., STEMPER, B., SCHLICK, M., PHILIPPENS, M., and WISMANS, J. (2000). Biomechanics of human occupants in simulated rear crashes: Documentation of neck injuries and comparison of injury criteria. Proc. 44th Stapp Car Crash Conference, SAE Paper No. 2001-01-SC14.

## DISCUSSION

PAPER: **An Experimental Seat for Measuring External Biofidelity in Rear Impacts**

PRESENTER: ***Yun Seok Kang, The Ohio State University***

**Q**UESTION: *Andrew Merkle, Johns Hopkins*
Interesting work. I'm curious as to the seatback parameters when you compare your results with a real-world impact where you don't have what I'm assuming are rigidly-mounted load cells. We've toyed with backing as well and we saw some significant differences when you look even at seat cushion stiffnesses. So if you could just talk to that point.

**A**NSWER: I'm not clear about your question.

**Q:** Your load cells are mounted in your seatback and your head restraint. So you said your future work, for example, would be looking at cadaver testing, etc. So, comparing your results: How may they differ if we were to use the basis of your results for future testing? You have a seat that's loaded with rigidly mounted load cells versus a compliant seat in the real-world environment. Could you just speak to potential difference? For example, lumbar loads that we saw were significantly different when we toyed with seatback properties.

**A:** Okay. Now we didn't prepare the PMHS test. We just focused on this load cell component, the load cell distribution loading and the seat loading also.

**Q:** Yeah.

**A:** Because we just focused on the internal biofidelity of the rear impact on an ATD, and we will compare. We will do the test using PMHS and then compare the PMHS test and the ATD response using this load cell compilation.

**Q:** Okay. Thanks.